Development of pneumatic human interface and its application for compliance display

Masahiro Takaiwa
Okayama University

Toshiro Noritsugu
Okayama University

Development of Pneumatic Human Interface and Its Application for Compliance Display

Masahiro Takaiwa
Faculty of Engineering
Okayama University
3-1-1 Tsushimanaka, Okayama, Japan
takaiwa@sys.okayama-u.ac.jp

Toshiro Noritsugu
Faculty of Engineering
Okayama University
3-1-1 Tsushimanaka, Okayama, Japan
toshiro@sys.okayama-u.ac.jp

Abstract

The goal of this study is to develop a human interface that can display compliance for human hand aiming at the application in the field of virtual reality. Pneumatic parallel manipulator is introduced as a driving mechanism of our human interface, consequently, which yields characteristic that the manipulator works as a kind of elastic body even when its position/orientation is under the control. Utilizing this elastic characteristic, a compliance display scheme is proposed. The validity of the proposed scheme is verified experimentally.

1 Introduction

Virtual reality technologies have become one of the recent attracts not only in the amusement field but also in the industrial one aiming at applying to, such as, the virtual prototyping in mechanical CAD or the surgery simulation[1]. Among the virtual reality technologies, the development of the instruments, which display the force or the tactile feeling, is important because such a feeling, besides of the vision, plays an important role for human to recognize an environment. Pneumatic actuators are effective for this kind of instruments[2][3] since its inherent features of softness and safety are indispensable for this kind of mechanical systems which contact with human directly.

In this paper, we aim at developing a human interface that can display compliance of virtual object for human hand by utilizing the characteristic of pneumatic driving system positively.

Concretely, Stewart type parallel mechanism is introduced to our human interface since it drives multiple d.o.f. for its compactness. Additionally pneumatic cylinder is employed as a driving actuator, which enables the human interface to work as a kind of elastic body even when position control is carried out owing to the air compressibility.

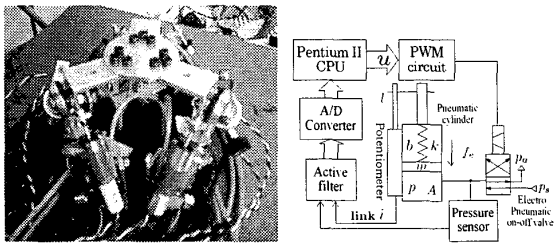

(a) Parallel Link Mechanism (b) Pneumatic Driving Circuit

Figure 1: Developed Human Interface

Positively utilizing this elastic characteristic compliance display scheme is proposed, where contact point and contact force are detected with no use of force/moment sensor[4] and a compliance control system is constructed based on such a detected information.

The validity of the proposed scheme is confirmed through some experiments and analysis.

2 Outline of Developed Human Interface

Fig. 1 (a) shows the parallel manipulator that works as a skeleton mechanism of our human interface. 6 pneumatic cylinders (10 mm in diameter and 15mm in stroke) are employed and they drive an upper platform in 6 d.o.f..

The position/orientation of the upper platform is described by a hand vector $\boldsymbol{h} = [x, y, z, \phi, \theta, \psi]^T$ where x, y, z are horizontal displacements and ϕ, θ, ψ expressed by roll-pitch-yaw angle indicate the posture. Similarly a link vector is defined as $\boldsymbol{\ell} = [\ell_a, ..., \ell_f]^T$ with an element of a displacement of each piston rod.

In the mean while, Fig.1 (b) shows the pneumatic driving circuit of one cylinder. The pressure in a head

0-7803-6456-2/00/$10.00 ©2000 IEEE

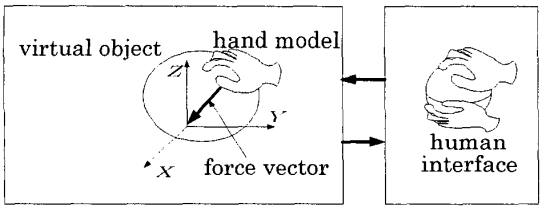

Figure 2: Concept of compliance display

side chamber of pneumatic cylinder p is regulated by on-off type electro magnetic valve driven by PWM method. The displacement of piston rod is measured by potentiometer and p is detected by a pressure sensor. A control signal u calculated every sampling period(10 ms) in a computer corresponds to a duty ratio of PWM. Supply pressure p_s=200kPa.

3 Realization of compliance display

3.1 Concept of compliance display

Fig.2 shows the conception idea of compliance display, which is realized as the following sequences.

1. Human holds the developed human interface by covering with his/her palm and gives force by one finger.
2. The human interface itself detects which finger applying force and how much that force is.
3. In virtual environment, desired compliance is refereed to based on the relative position between a corresponding finger in the hand model and the virtual object.
4. The human interface displays that compliance to the direction of the finger by constructing compliance control system.

The detection of the finger is done by that of the contact point. After mentioning the detection scheme of the contact point and the contact force based on an elastic characteristic of the position servo mechanism, compliance display method using these detected force information is described in the below.

3.2 Position control system

Fig.3 shows the proposed position control system[5]. A variable with upper-case letter represents *Laplace* transformed variable vector one and (s) is neglected for simplicity and the transfer function in a block shows one element of the diagonal matrix, where each parameter is represented in TABLE 1.

Table 1: System parameters

ℓ	displacement of piston rod
p	pressure in head side
A	effective sectional area of chamber
ω_n	natural frequency
ζ	damping coefficient
T_q	time constant of filter Q
m	equivalent mass including that of piston rod
m_n	nominal model of m
b	damping coefficient
b_n	nominal model of b
k	spring coefficient
f_e	total amount of external force (coulomb friction, interaction force etc.)

This control system is designed so that its closed loop transfer function may be approximated by the following desired 2nd order system.

$$\begin{aligned} H &= G_r H_d \\ &= \mathrm{diag}\left\{ \frac{\omega_{ni}^2}{s^2 + 2\zeta_i\omega_{ni}s + \omega_{ni}^2} |_{i=x,y,\ldots,\psi} \right\} H_d \quad (1) \end{aligned}$$

Modifying Eq.(1), the desired velocity of hand coordinate variables sH_d is obtained through the controller C_1 and it is translated into desired velocity of piston rod sL_d through *Jacobi* matrix J which is derived as the following relation.

$$\frac{d\boldsymbol{\ell}}{dt} = J(h)\frac{d\boldsymbol{h}}{dt} \quad (2)$$

In a parallel manipulator, contrary with a serial one, $\boldsymbol{h}$ can not be obtained analytically. In this study convergence calculation(*Newton -Raphson* method) is employed to obtain $\boldsymbol{h}$ at every sampling period and its sufficient convergence accuracy has been confirmed.

Subsequently a velocity control system is constructed based on the pressure control system by introducing a disturbance observer[6], where spring element is treated as disturbance from the designing policy of the controller. C_2 is a phase lead transfer function to cancel the transfer characteristic from the output of C_2 to sL, which satisfy Eq.(1).

3.3 Detection of Contact Point and Contact Force

From Fig.3 closed loop relation from the output of J to sL is simply described as

$$F_e = I_{mp}(sL_d - sL) \quad (3)$$

under the assumption C_2 cancels the transfer characteristic from the output of C_2 to sL. In Eq.(3), I_{mp}

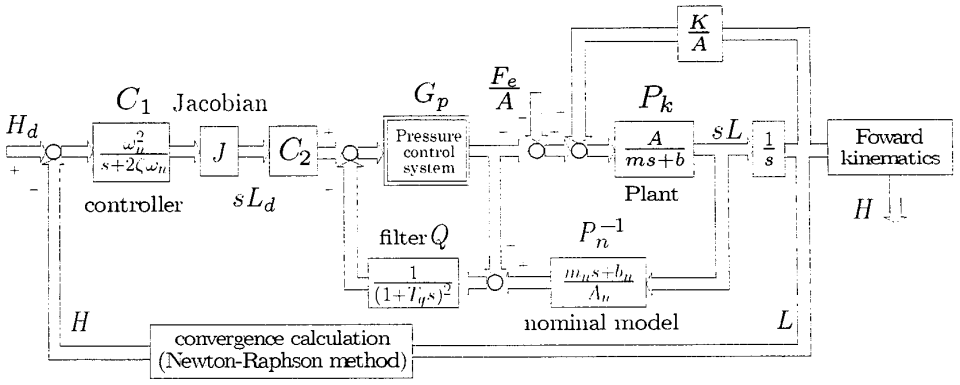

Figure 3: Position control system

corresponds to a mechanical impedance per one link, which is represented as a form of

$$I_{mp} = AG_pC_2(I - QG_p)^{-1} \tag{4}$$

where G_p is a closed loop transfer function of inner pressure control system.

In pneumatic systems, $|I_{mp}|$ becomes small in the low frequency range. This is one of the reasons why it is not easy to improve a positioning accuracy in pneumatic system since inverse of I_{mp} is equivalent to a sensitivity function. However this characteristic yields the compliance (softness) which must be indispensable for the human friendly mechanical systems including a human interface in this study.

From a principle of virtual work, a force/torque applied at an origin of $\boldsymbol{h}$, $\boldsymbol{f}_m = [f_{mx}, f_{my}, f_{mz}, \tau_{m\phi}, \tau_{m\theta}, \tau_{\psi}]^T$ is related with a force vector equivalently acting on a link $\boldsymbol{f}_e$ through *Jacobi* matrix as

$$\boldsymbol{f}_m = J^T \boldsymbol{f}_e \tag{5}$$

Substituting *Laplace* transformed Eq.(5) into Eq.(3) by considering Eq.(2), yields eq.(6)

$$\begin{aligned} F_m &= J^T I_{mp}(sL_d - sL) \\ &= J^T I_{mp} J C_1 G_r^{-1}(G_r H_d - H) \end{aligned} \tag{6}$$

In right hand side, $J^T I_{mp} J C_1 G_r^{-1}$ corresponds to mechanical impedance of manipulator. Eq.(6) shows that if mechanical impedance of link I_{mp} is known then force/torque F_m considered at an origin of $\boldsymbol{h}$ can be estimated without using a general force/moment sensor.

In order to detect contact force and contact point based on the F_m calculated in Eq.(6), we reset hand coordinate system so that $J^T J$ in Eq.(6) becomes (almost) diagonal matrix at its origin. In generally such an origin is called "compliance center". Additionally

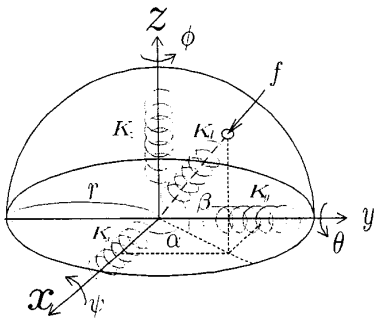

Figure 4: Geometrical model

a hemispherical shell is newly introduced so that its center point match to the origin of h (namely to the compliance center).

Fig.4 shows a geometrical model, where contact point of force vector $\boldsymbol{f}$ is expressed by polar coordinates (r, α, β) and $\boldsymbol{f}$ is assumed to apply along with a normal direction for the surface of hemispherical shell.

As you see that, force vector $\boldsymbol{f}$ is simply derived from the balance of translational force around the origin by using the first 3 elements in $\boldsymbol{f}_m$ as

$$\boldsymbol{f} = [f_{mx}, f_{my}, f_{mz}]^T \tag{7}$$

On the other hand, the contact point (r, α, β) is expressed as Eq.(8) since no moment is generated around the origin owing to the physical characteristic of compliance center.

$$\alpha = \tan^{-1}(\frac{f_{my}}{f_{mx}}), \beta = \tan^{-1}(\frac{f_{mz}}{\sqrt{f_{mx}^2 + f_{my}^2}}) \tag{8}$$

In our manipulator, a compliance center was found to be at 4.6 mm upon the center of the bottom plane and the $J^T J$ at that point is represented as follows, where non-diagonal elements are represented by 0 since

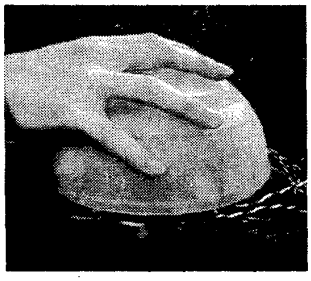

Figure 5: Manipulator covered by shell

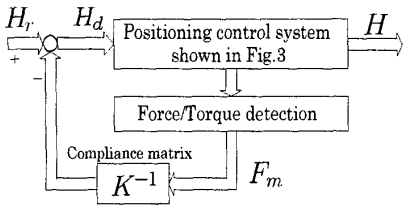

Figure 6: Compliance control system

they are significantly negligible compared to the diagonal one.

$$J^TJ = \begin{bmatrix} 0.9 & 0 & 0 & 0 & 0 & 0 \\ 0 & 0.9 & 0 & 0 & 0 & 0 \\ 0 & 0 & 4.2 & 0 & 0 & 0 \\ 0 & 0 & 0 & 4.9\times10^3 & 0 & 0 \\ 0 & 0 & 0 & 0 & 5.6\times10^3 & 0 \\ 0 & 0 & 0 & 0 & 0 & 5.6\times10^3 \end{bmatrix} \quad (9)$$

Hence a hemispherical shell is mechanically attached to the skeleton parallel manipulator so as to make its center to match the compliance center, which is shown in Fig.5.

The shape of hemispherical shell, off course it plays an important role in the detection scheme analytically, can also be said to be a human friendly shape from a view in an ergonomic meaning.

3.4 Compliance display

In order to display compliance to the contact point (namely finger which applied force), compliance control system shown in Fig.6 is constructed.

Detected contact force F_m is fed back through the compliance matrix K^{-1}=diag$\{K_x^{-1},K_y^{-1},K_z^{-1},0,0,0\}$ and position control system shown in Fig.3 is constructed.

The remaining problem is how much each element K_x, K_y, K_z should be set to realize the desired compliance given for the arbitrary direction.

From Fig.4, balance of translational force at the origin of $\boldsymbol{h}$, the relation between the desired stiffness K_d for the direction of the contact point (r,α, β) and the stiffness for each axis is represented as follows.

$$K_d = \sqrt{(K_x\cos\alpha\cos\beta)^2 + (K_y\sin\alpha\cos\beta)^2 + (K_z\sin\beta)^2} \quad (10)$$

In order to fix the value of K_x, K_y and K_z which satisfy Eq.(10), we introduce an constrained condition that the compliance control characteristic should be normalized for each direction.

On the Fig.6, next relation is easily obtained.

$$H_r - K^{-1}F_m = H_d \quad (11)$$

Substituting Eq.(11) into Eq.(6) to cancel H_d, the compliance control performance is represented as the following equation.

$$F_m = RG_r^{-1}(G_rH_r - H) \quad (12.a)$$

$$\text{where } R = I_{mp}J^TJC_1(I + I_{mp}J^TJC_1K^{-1})^{-1} \quad (12.b)$$

Seeing from Eq.(9), diagonal element corresponding to the z axis in J^TJ is almost 4 times as much as that for x and y axis. Therefore by setting each element of K according to the ratio in Eq.(13), the dynamics of the compliance control characteristic for x, y, z direction (namely each diagonal element for x, y, z direction of R in Eq.(12.a)) becomes equivalent except for the influence of a static gain.

$$K_x : K_y : K_z = 1 : 1 : 4 \quad (13)$$

Substituting Eq.(13) into Eq.(10), each of the stiffness is given as

$$K_x = \frac{K_d}{\sqrt{1 + 15\sin^2\beta}} \quad (14)$$

$$K_y = \frac{K_d}{\sqrt{1 + 15\sin^2\beta}} \quad (15)$$

$$K_z = \frac{4K_d}{\sqrt{1 + 15\sin^2\beta}} \quad (16)$$

Fig.7 shows the frequency characteristic of the term R in the right hand side of Eq.(12.a).

By normalizing the frequency characteristic of the compliance control performance for each axis, the frequency characteristic of the desired compliance(admittance) can be also prescribed by the same frequency characteristic, which is useful in evaluating the realization of the desired compliance(admittance) in a frequency domain.

4 Experiments and Discussion

4.1 Position control performances

Fig.8 shows the positioning step response, where (a) and (b) corresponds to the horizontal and rotational

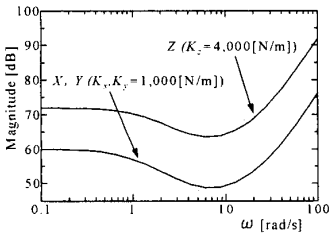

Figure 7: Frequency characteristic

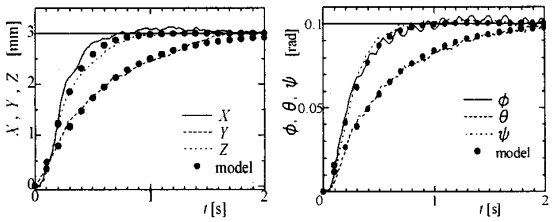

(a) Horizontal direction (b) Rotational direction

Figure 8: Position control performance

direction, respectively. • indicates the response of a model shown in Eq.(1). For all direction, ω_n and ζ are set to 8.0 [rad/s] and 1.0, respectively except that ζ for y and θ direction is intentionally set twice as much as that of the other direction.

The obtained responses for each direction are almost the same with that of the desired model, which proves an effectiveness of a proposed position control system.

4.2 Estimation of force on link

Before discussing on the compliance display, the estimation performance of the force applied on the link is investigated.

Fig.9(a) shows the frequency characteristic of the mechanical impedance of a link I_{mp}, where • and dotted line indicate the result of the identification obtained from experiment and that calculated from Eq.(4), respectively. It is essential to use Eq.(4) in the implementation, but an approximated model of the following form is employed for simplicity, which is shown by the solid line in the figure.

$$I_{mp} = \frac{K_i(1+T_2 s)^2}{s(1+T_1 s)} \qquad (17)$$

, where$K_i = 4.6 \times 10^2$ [Ns/m], $T_2 = 0.047$ [s] and T_1 is set enough small only to guarantee a proper characteristic.

Fig.9(b) shows the estimation performance of the force applied on a link. It is confirmed that the estimated force using Eq.(3)(solid line) agrees approx-

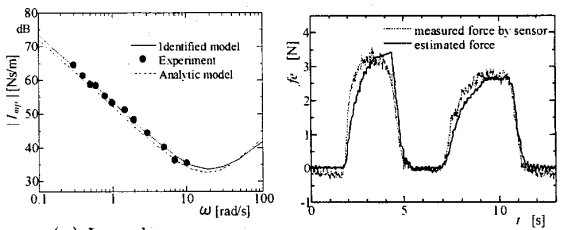

(a) Impedance characteristic (b) Force estimation

Figure 9: Estimation performance of force applied on link

imately with the force measured by a sensor (dotted line), which prove the effectiveness of the proposed detection scheme of contact force and the approximation of I_{mp}.

4.3 Compliance display performance

Fig.10 shows the control performances of the compliance display.

First of all, contact force $\boldsymbol{f}$ is applied along with normal direction for the surface of the hemispherical shell through a force sensor at the point of α=-120 deg. and β=60 deg. as shown in figure (a) at the state of the compliance control system has been carried out with $H_r = 0$. The displaying performances have been done similarly for 2 cases when the reference stiffness of K_d=5 [N/mm] and K_d=2 [N/mm], whose results are corresponding to the left 3 figures numbered by (i) and the right 3 numbered by (ii), respectively through the figure (b),(c) and (d).

The figure (b) shows the estimation performance of the contact point based on the Eq.(8). The contact point is estimated when the norm of estimated force $|\boldsymbol{f}|$ exceed a certain value (2 [N]). Subsequently figure (c) displays the estimation performance of contact force, where solid line and the dotted one are the norm of the estimated force $|f|$ and the force measured by a force sensor, respectively. In the last figure (d), realization of the desired compliance is evaluated by comparing the desired force $K_d|Hr - H|$ shown in the solid line with the force measured by force sensor shown in the dotted line.

In the case that K_d is set to rationally large 5 [N/mm], almost satisfactory performances are confirmed commonly in estimating the contact point/contact force and in realizing the desired compliance. It is not mentioned in this paper but almost the same control performances for the same K_d were also obtained for any other contact point, which proves the possibility to display compliance feeling to an arbitrary finger.

However in the case that K_d is set to 2 [N/mm],

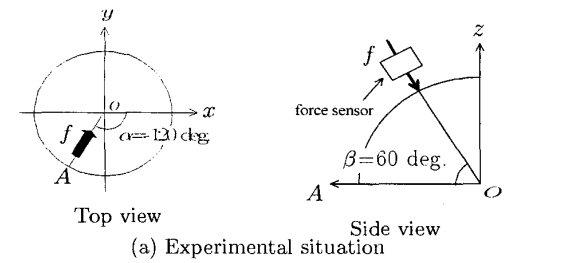

(a) Experimental situation

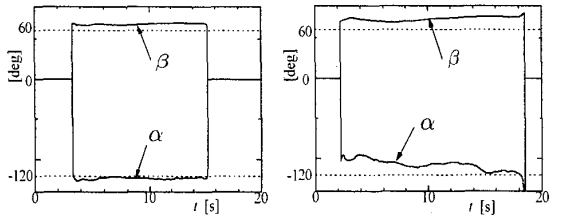

(i) K_d=5 N/mm (ii) K_d=2 N/mm

(b) Evaluation of contact point

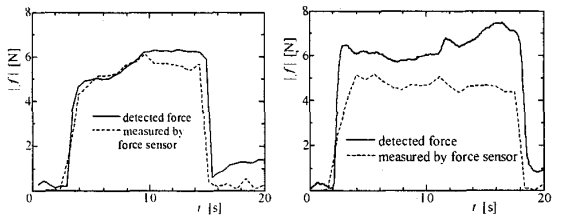

(i) K_d=5 N/mm (ii) K_d=2 N/mm

(c) Evaluation of contact force

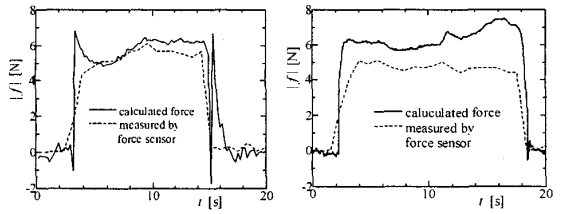

(i) K_d=5 N/mm (ii) K_d=2 N/mm

(d) Evaluation of compliance

Figure 10: Compliance display performance

namely the case to display more soft object, it can be confirmed the control performance get worth. It is mainly resulted from the decrease of estimation accuracy of contact force since our compliance display scheme is entirely dependent on the precise estimation of the contact force. The reason why the estimation accuracy is lowered against the low stiffness is currently under the investigation.

5 Conclusion

In this study, we developed a human interface, in which a pneumatic parallel manipulator is employed as its driving mechanism, aiming at displaying a compliance characteristic of a virtual object for human hand.

In order to implement such an action, we proposed a compliance display scheme through the realization of the functions which estimate the contact point (which finger applied force ?) and contact force (how much is that force ?) with no use of force/moment sensor by positively utilizing the manipulator's elastic characteristic resulted from the air compressibility.

The validity of the proposed scheme was verified experimentally. The control performances of compliance display, namely the estimation accuracy of contact point and contact force, tend to get worth as the desired compliance is set larger. There is still room for further improvement of the estimation accuracy. Additionally the quantitative evaluation between the estimation accuracy error and the compliance recognition of the virtual object is also remaining as the future task.

Acknowledgement

We appreciate here to Industrial Technology Center of Okayama Prefecture for their cooperation in making the hemispherical shell.

References

[1] R.Baumann, R.Clavel, *Haptic Interface for Virtual Reality Based Minimally Invasive Surgery Simulation*, Proc. IEEE ICRA, 381/386, 1998

[2] Y.Tanaka, T.Kikuchi, A.Kaneko, *Force Display in Virtual World by Fluid Power Glove*, Proc. of the Fourth JHPS Int. Symp. on Fluid Power, 187/192, 1999

[3] Y.Tanaka,T.Kanamori, *Dynamic Force Display Device by Pneumatic Pressure Control*, Proc. of Fifth Triennial Int. Symp. on Fluid Control, Measurement and Visualization, vol.2, 719/723, 1997

[4] M. Takaiwa *and* T. Noritsugu, *Development of Human-Robot Haptic Interface Using Pneumatic Parallel Manipulator*, Proc. of the Fourth JHPS Int. Symp. on Fluid Power, 181/186, 1999

[5] T. Noritsugu *and* M. Takaiwa, *Motion Control of Pneumatic Parallel Manipulator Using Disturbance observer*, Japan-U.S.A. Flexible Automations, 1986.

[6] T. Murakami *and* K. Ohnishi, *Advanced Control Technique in Motion Control*, The Nikkan Kogyo Shinbun Ltd., Japan, 1990